RSC Advances

ROYAL SOCIETY OF CHEMISTRY

www.rsc.org/advances

TOC

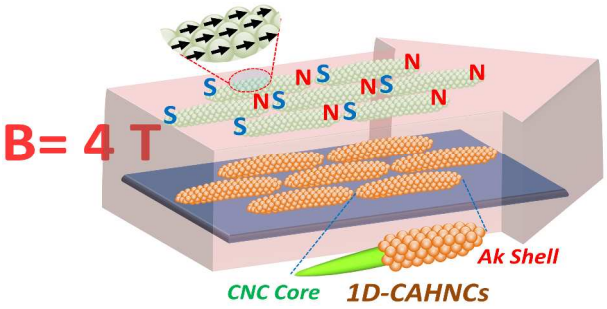

Magnetic field induced self-assembly of the synthesized one-dimensional core-shell cellulose-akaganeite hybrid nanocrystals (1D-CAHNCs).

RSC Advances

RSCPublishing

ARTICLE

One-Dimensional Core-Shell Cellulose-Akaganeite Hybrid Nanocrystals: Synthesis, Characterization, and Magnetic Field Induced Self-Assembly

Cite this: DOI:

Received,
Accepted

DOI:

www.rsc.org/

Mahdi Mashkour,[a] Tsunehisa Kimura,[b] Fumiko Kimura,[b] Mozhdeh Mashkour[a] and Mehdi Tajvidi[c] ,

Cellulose akaganeite hybrid nanocrystals (CAHNCs) were made by in situ synthetizing of spherical akaganeite nanoparticles in the presence of pre-oxidized cellulose nanocrystals as a reducing agent for the reduction of dissolved ferrous ions under heat treatment and neutral gas flow. Characterization of the produced nanostructures by means of field emission scanning electron microscopy (FESEM), X-ray diffraction (XRD), attenuated total reflection–Fourier transform infrared (ATR-FTIR) spectroscopy, and vibrating sample magnetometry (VSM) confirmed that the fabricated one-dimensional nanoparticles were composed of a rodlike cellulose nanocrystal cores coated by shells of spherical chloride-containing akaganeite nanoparticles with an average diameter of about 4-6 nanometer and superparamagnetic property. To compare magnetic response of the synthetized CAHNCs with the starting diamagnetic CNCs, static magnetic fields of 1, 2, 4, and 8 T generated by a superconducting magnet were applied to suspensions of either material during dewatering process. In contrast to the CNCs, the CAHNCs were well aligned under a magnetic field intensity of 4 T and above. Also, magnetic susceptibility of the CAHNCs was different from CNCs by exhibiting magnetic field induced self-assembly parallel to the external magnetic field direction. Cellulose akaganeite hybrid microcrystals (CAHMCs) were added to the system as micro-scale models, also confirmed the magnetic field induced self-assembly. Polarizing optical microscopy, FESEM, and wide-angle X-ray diffraction (WAXD) strongly confirmed unidirectional magnetic field induced self-assembly of the CAHNCs parallel to the external magnetic field even under 2 T magnetic intensity. Reasons behind these observations are extensively discussed.

INTRODUCTION

One-dimensional organic-inorganic core-shell hybrid nanostructures (1D-OICSHNSs) have recently attracted a lot of attention because of their outstanding geometry and size dependent physicochemical and mechanical properties.[1-3] Promising potential applications of these heterostructure nanomaterials in modern high-tech industries and research fields related to designing and fabricating advanced functional materials such as high-performance super capacitors, batteries and solar cells, photo catalysts, self-cleaning surfaces, smart and anti-corrosive coatings, sensors, electronic devices and electromagnetic absorbers have encouraged material scientists to focus on synthesis and characterization of these nanomaterials.[3-6] The intriguing properties of the synthesized OICSHNSs are derived from a synergistic combination of properties of both the organic core and the inorganic shell components.[6] Using polymeric materials as the core part of the heterostructure nanoparticles has some significant advantages such as lighter final products, easier processability, the possibility to remove the core and the availability of a vast variety of polymers with different properties tailored for the final desired performance.[2, 7] High specific surface of the polymeric nanoparticles having surface-active functional groups can provide an appropriate substrate for nucleation and controlled growth of desired inorganic nanoparticles and formation of the OICSHNSs. Reportedly, functionalized polystyrene and latex are the most prominent polymers used as the core part of the OICSHNSs.[8-11] To our best knowledge there

is no successful report on fabricating zero or one-dimensional OICSHNSs based on cellulose nanocrystal (CNC) core, while, the outstanding physicochemical and mechanical properties of the CNCs have been well known for more than two decades. The rod-like shaped CNCs have recently attracted a great deal of attention for advanced applications in the fields of composite materials, optic and electronic industries, aerospace engineering and medicine.[12, 13] Having a low density (~1.6 g/cm^3) versus a very high stiffness (~140 GPa) and strength (~10 GPa), high surface to volume and aspect ratios, very low coefficients of thermal expansion and biocompatibility are some of the most promising unique properties that showcase the CNCs as advanced materials for the future.[13, 14] These excellent and unique properties and on the other hand, a highly reactive and readily functionalizable surface, inherently densely covered with hydroxyl (-OH) functional groups candidate the CNCs as a promising high potential material for fabricating novel 1D-OICSHNSs.[13, 15] Here, for the first time, the successful synthesis of highly purified 1D-OICSHNSs with a CNC core and akaganeite (β-FeOOH) nanoparticle shell prepared with a facile green chemical surface functionalization and modification process is reported. Although the first fabrication of iron oxide nanoparticles covered cellulose long fibers dates back to about two decades ago and some successful trials have been reported in the meantime,[16] some of the processing challenges such as low efficiency and difficulties in purification and separation of the byproducts seem to have hindered successful preparation of the CNC core based 1D-OICSHNSs.
Magnetically, due to the lack of the intrinsic magnetic dipoles, cellulose, like most of the other polymers, is known as a feeble diamagnetic material meaning that cellulose is magnetically actuated only when it is affected by a strong external magnetic field often produced by superconducting magnets.[17, 18] Depending on the type and situation of the structural covalent bonds, the anisotropic diamagnetic susceptibility of the polymeric materials can be positive or negative.[18-20] The anisotropic cellulose diamagnetic susceptibility is negative meaning that the cellulose chains align perpendicular to the direction of the strong enough static magnetic field.[14, 21, 22] Also, with decreasing the size of diamagnetic materials from micro to nanoscale, the external magnetic field strength should be increased to overcome the thermal energy and other physical phenomena that may negatively affect the magnetic alignment of the diamagnetic nanoparticles.[19, 20] That is why some researchers have reported external magnetic field strengths up to 20 T for well-aligning the CNCs.[23] Regardless of the high cost of the consumed energy and supplying and maintaining such facilities that can provide these strong magnetic fields, the harmful effects of such strong magnetic fields on the health of the human and environment are well known.[24] By using the method that we report here, fabricating novel 1D-OICSHNSs based on CNCs with a vast variety of different physicochemical properties and potential applications will be possible. Although here we focused on fabricating a cellulose core magnetic shell nano-heterostructure that well responses to much weaker modulated external magnetic fields with a positive magnetic susceptibility, the authors believe that the explained method opens new windows to making novel 1D-OICSHNSs consisting of cellulose nanocrystals and a vast variety of functional metal oxides with unique and outstanding properties to be used in modern high-tech industries and medicine.

EXPERIMENTAL SECTION

Materials

Whatman CF-11 fibrous cellulose powder (Catalogue No. 4021050) was used as starting cellulose material for extraction of cellulose nanocrystals. Hydrobromic acid (HBr), ferrous chloride tetrahydrate ($FeCl_2{\cdot}4H_2O$ > 99%) and hydrogen peroxide (H_2O_2, 30% v/v) were purchased from Nakalai Tesque, INC. (Kyoto, Japan) and used without further purification.

Extraction of Cellulose Nanocrystals

Rod-like cellulose nanocrystals (CNCs) were prepared by hydrobromic acid hydrolysis of CF-11 cellulose powder. Acid hydrolysis was performed in 3 N HBr for 4 h at 100 °C in a 3-neck, round bottom flask fitted with a thermometer, a reflux condenser and a magnetic stirrer. To quench acid hydrolysis, dilution was done two times and the diluted acidic suspension was then centrifuged by a high speed centrifuge (Tomy Seiko Co. Ltd., model CM-60RN) at 10,000 rpm for 15 min. This step was repeated 3 times and each time the supernatant acidic solution was removed and replaced with distillated water. After that, the white color suspension was sonicated for 10 min at 24 kHz using an ultrasonic lab homogenizer UP400S (Hielscher Ultrasonics, GmbH, Germany) to break down agglomerated cellulose microparticles to individual nanoparticles and increase the final yield. The sonicated suspension was then poured into a Fisherbrand dialysis tubing (Thermo Fisher Scientific Inc., Catalog No. 21-152-8) and dialyzed against distillated water for 12 days at room temperature. After neutralization, to separate the CNCs, the suspension was centrifuged again for 15 min at 10,000 rpm. This step was repeated to obtain a turbid supernatant containing individual CNCs. The supernatant was poured into lab glassware and stored at 4 °C until used. Also, the precipitated cellulose microcrystals (CMCs) obtained in the last step of centrifugation were separately stored to be used later.

Preparation of Cellulose-Akaganeite Hybrid Nanocrystals

To prepare cellulose-akaganeite hybrid nanocrystals (CAHNCs), first the CNCs were partially oxidized by using hydrogen peroxide (H_2O_2) as one of the known cellulose oxidizing agents. To oxidize CNCs, 100 ml of H_2O_2 (30% v/v) was added to 50 ml of a 0.5% CNC suspension under slight magnetic stirring. The glass container containing the suspension was carefully capped and covered by a piece of parafilm and aluminum foil, respectively and it was allowed to be stirred for 24 h at room temperature. The oxidized CNC suspension was

then centrifuged at 12000 rpm for 15 minutes to remove the excess H_2O_2 and refine the oxidized CNCs (OCNCs). The white color solid residue was resuspended by adding 100 ml of distillated water and one more time it was centrifuged. After removing the supernatant, the precipitated OCNCs were diluted again to 100 ml. To prevent undesirable oxidation of Fe^{2+} (iron) ions by excess dissolved oxygen molecules, deoxygenating was carried out by bubbling nitrogen through the suspension for at least 1 h before adding the iron salt. To supply the Fe^{2+} ions, 1 M ferrous chloride tetrahydrate ($FeCl_2$. $4H_2O$) was added to the OCNCs suspension under magnetic stirring and nitrogen gas flow was maintained. Immediately after adding Fe^{2+} ions, an exothermic reaction occurred and the color of the suspension turned from milky white to orange while pH decreased down to 1. After 45 min, to neutralize the suspension and remove the extra unreacted Fe^{2+} ions, the resultant chemically modified CNCs were washed for several times by centrifugation at 10000 rpm for 10 min. The described method, was also used to chemically modify the previously prepared CMCs. The explained preparation procedure is illustrated step by step in Scheme 1.

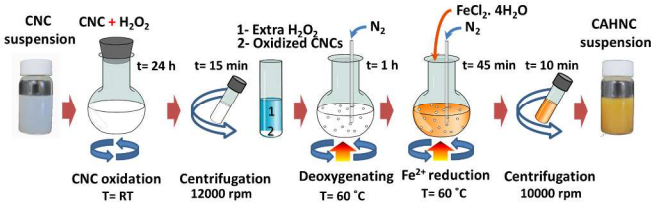

Scheme 1. Step by step schematic representation of the fabrication process of the CAHNCs.

Magnetic Response Investigation

To investigate and compare magnetic responses of the prepared CNCs and the CAHNCs, a cryocooler cooled superconducting magnet (SHI, Sumitomo Heavy Industries, Ltd.) was used to generate horizontal static magnetic fields of 1, 2, 4 and 8 T. Several drops of the 0.05% solution of the CNCs and CAHNCs were dropped on glass slides and then the glass slides were placed in the center of the magnet bore and the liquid phase was allowed to evaporate. After the liquid was completely evaporated, the residual solid thin layers were characterized using different techniques.

Characterization

Recognition of the made hybrid nanocrystal structures was carried out by an X'Pert Pro MPD X-ray diffractometer equipped with a PIXcel detector (PANalytical BV, The Netherlands) at 40 kV and 40 mA using Ni-filtered Cu Kα radiation at a wavelength λ = 1.5418 Å in the range 2θ = 10 – 70°. XRD data were collected by step scanning with a step size of 0.026° 2θ and a scan step time of 78.8 s. The collected data were analyzed using the X'Pert HighScore Plus software package. Also, to investigate the magnetic alignment of the synthesized hybrid nanoparticles, 2D wide angle X-ray diffraction (WAXD) patterns were recorded using a Rigaku RINT-2000 diffractometer (Rigaku LTD, Japan) with Cu Kα radiation (λ = 1.5405 Å) at 40 kV and 40 mA.

Infrared spectroscopy was carried out using a Perkin Elmer Frontier spectrophotometer (PerkinElmer, Waltham, MA, USA) equipped with a universal ATR sampling accessory in the range of 400 to 4000 cm^{-1} at a 1 cm^{-1} resolution.

Magnetization measurements were performed using a Lakeshore Model 7400 vibrating sample magnetometer (VSM) at room temperature.

The morphology and alignment of the produced nanocrystalline hybrid structures were characterized by means of a Hitachi S-4800 field emission scanning electron microscope (FESEM; S-4800, Hitachi Ltd., Tokyo, Japan) operating at low accelerating voltages of 1.5 kV to 5 kV. To avoid charging effect on the sample surface during scanning electron microscopy observation, surfaces of all samples were sputter coated with platinum (Pt) using an ion-sputtering coater Hitachi E-1045 (Hitachi Ltd., Tokyo, Japan). The alignment of CNCs and CAHNCs under modulated external magnetic field was quantitatively assessed using the OrientationJ plugin (Biomedical Image Group, Ecole Polytechnique Federale De Lausanne, Switzerland) of ImageJ software (ver. 1.48, US National Institutes of Health, USA) and OriginPro 9.1 (OriginLabs, Northampton, MA, USA).

To observe and compare the quality of the magnetic alignment, polarized light microscopy (PLM) micrographs were obtained using a Nikon Labophot 2-Pol polarizing transmitted light microscope (Nikon, Tokyo, Japan). To quantify the qualitative results of the PLMs, an innovative method was used. The changes in values of contrast intensity of the colors, red, green, and blue (RGB) for two deflection angles of +45° and -45° with respect to the external magnetic field direction were assessed using the ImageJ software. A relative color contrast value (RCC) belonging to each sample affected by a specific strength of the external modulated magnetic field was calculated according to Equation (1):

$$RCC_{i_{j_r}} = \frac{\left|CI_{(ij)_{+45°}} - CI_{(ij)_{-45°}}\right|}{\left|CI_{(ir)_{+45°}} - CI_{(ir)_{-45°}}\right|} \quad (1)$$

where, CI, i , j, and r stand for the color intensity, complementary color, applied and reference magnetic field intensities, respectively. Therefore, the relative color contrast value or its abbreviated $RCC_{i_{j_r}}$ is defined as a ratio between the differential i color intensity (CI) resulted by changing deflection angle of 90° between +45° and -45° with respect to the direction of a certain magnetic field intensity (j) and its differential values under a reference magnetic field intensity. The calculated RCC values were used to compare the improvement of magnetic response of the produced CAHNCs versus the initial CNCs.

RESULS AND DISCUSSION

Morphology and Structural Properties

Morphology, size and microstructure of the CNCs and CAHNCs were examined using a FESEM. Figure 1a and 1b show micrographs of the rodlike CNCs extracted by acidic hydrolysis as described in the experimental section. Average length and diameter of the CNCs were determined to be 175 and 13 nm, respectively, which indicate an aspect ratio of about 13.5. FESEM micrographs obviously show changes on the surface of CNCs after chemical modification procedures were applied on the starting CNCs turning them to the final CAHNCs (Fig. 1c to 1e). Spherical nanoparticles with an average diameter of about 8±3 nm can be seen on the surface of CNCs. Micrograph 1e confirms that the spherical nanoparticles have densely covered the CNCs, so that the CNCs are fully encapsulated within the synthesized spherical inorganic nanoparticles. Hence, this new hybrid crystalline structures are composed of an organic core of CNC covered by an inorganic shell of spherical nanoparticles. Figure 1f shows the size distribution of diameters of the starting CNCs and the synthesized CAHNCs. As can be seen, the applied chemical modification procedures increased the average diameter of CNCs of about 13 nm related to the made inorganic shell. On the other hand, these micrographs show no extra and free spherical inorganic nanoparticle can be found among the made 1D crystalline hetrostructures and this point is a very important advantage, because selectively removing the extra nanoparticles and purification of the CAHNCs can be a big limiting challenge. Figure 1g schematically shows the structure of the synthesized 1D CAHNCs.

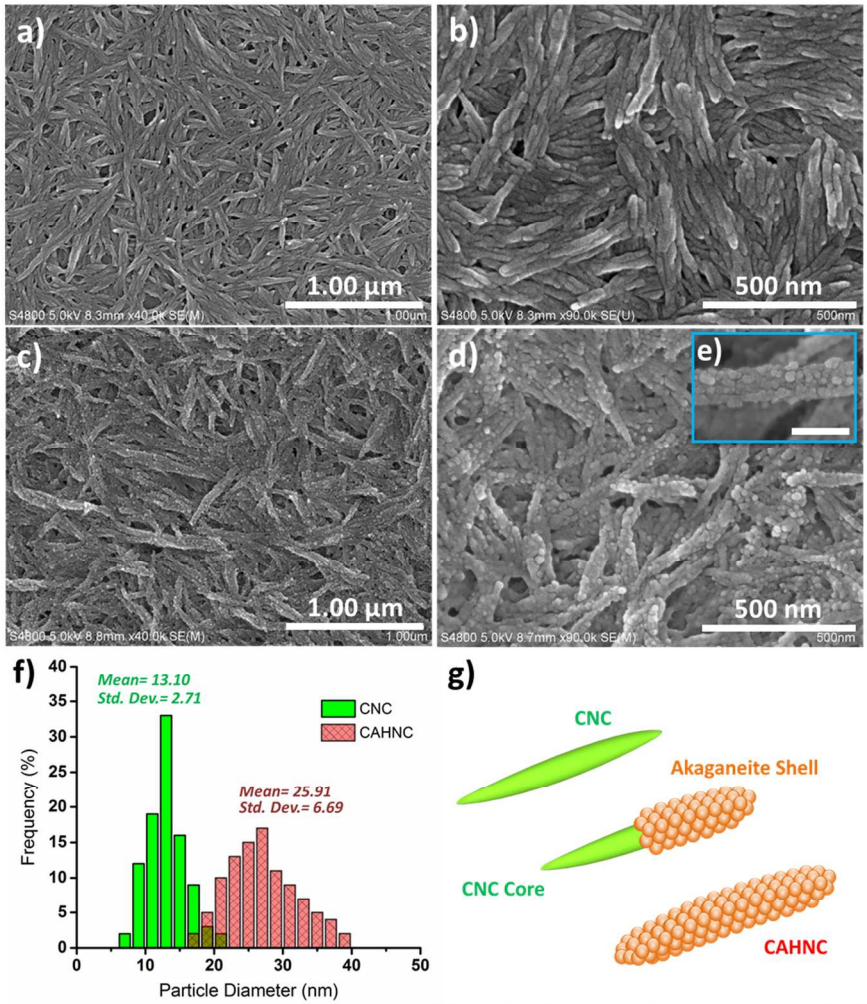

Figure 1. FESEM micrographs of the extracted CNCs (a and b), the synthetized CAHNCs (c and d), and a part of surfaces of a single CAHNC (scale bar is 30 nm) (e). Particle size distribution of the CNCs and CAHNCs (f). Schematic of core-shell structure of the CAHNCs (g).

Figure 2 shows XRD pattern for the produced 1D hybrid nanoparticles. As this figure shows, all of appeared peaks match well with the akaganeite-M (iron oxide chloride hydroxide) with I2/m monoclinic space group and lattice constants a = 10.60 Å, b = 3.035 Å, c = 10.51 Å, α and γ= 90.00°, and β= 90.22° referred to in the JCPDS card no. 42-1315 and no impurity peak can be detected. Also, as can be seen, the cellulose peaks at 16.48° and 34.32° overlap with the akaganeite peaks one at 17.05° and two other very close peaks at 34.41°, 35.22° making them undiscernible from each other.

The Scherer' equation was used to estimate crystallite size of the synthesized akaganeite nanoparticles and it was revealed that the average size of the spherical akaganeite nanocrystals was about 4-6 nm. Therefore, the FESEM and XRD findings confirmed that synthesis of the 1D crystalline heterostructure of CAHNCs was successfully carried out.

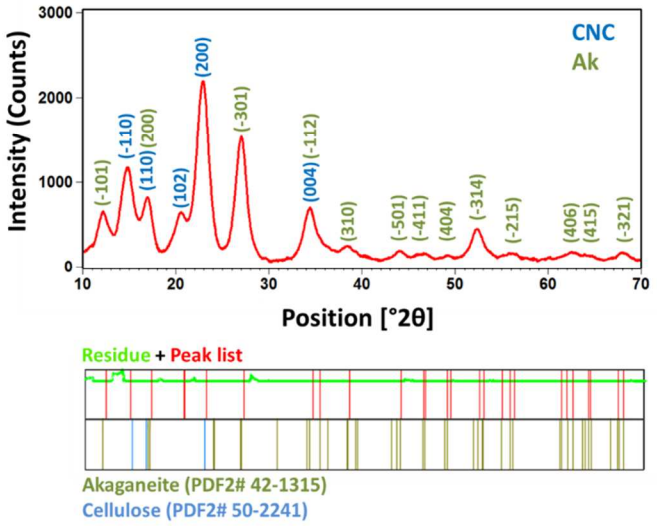

Figure 2. X-ray diffraction pattern of the synthetized CAHNCs.

To have a better understanding of the structural properties of the synthetized CAHNCs, ATR-FTIR was performed. Figure 3a and 3b show the ATR-FTIR spectra of CNCs and CAHNCs. As seen, turning the CNCs to the CAHNCs induced some changes in the spectra. Observation of two absorption peaks at around 695 and 847 cm^{-1}, which are due to the deformation vibration of the two O–H…Cl hydrogen bands confirm successful synthetizing of the chloride-containing akaganeite nanoparticles.[25] Also, appearance of two other peaks at around 420 and 474 cm^{-1} is attributed to the symmetric Fe–O–Fe stretching vibrations.[26-28] On the other hand, existence of an OH-stretching broad band with a maximum at 3345 cm-1 can also be attributed to the akaganeite structure. The bands at 1630 cm-1 in the CAHNC and CNC spectra correspond to absorbed H_2O in the CAHNC and CNC. The band at around 1548 cm-1 in the CAHNC's spectrum, in general, is assigned to COO- stretching band.[29] Thus, all of the obtained data from the FESEM, XRD, and ATR-FTIR strongly confirm the synthetized hetero-nanostructures were composed of an organic rodlike core of cellulose and a mineral shell made of spherical nanoparticles of the chloride-containing akaganeite.

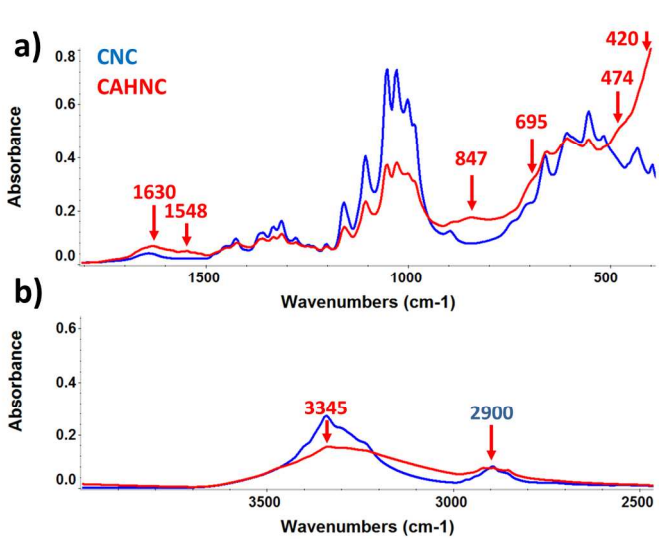

Figure 3. ATR-FTIR spectra of the CNCs and CAHNCs between a) 400 cm^{-1} to 1800 cm^{-1} and b) 2450 cm^{-1} to 4000 cm^{-1}.

Magnetic Response and Properties

Polarized light microscopy (PLM) images obviously indicate different magnetic behaviors of the starting CNCs and the produced CAHNCs after being subjected to magnetic fields upon drying (Figure. 4a to 4d). The CMCs and CAHMCs (10 percent w/w) were also added to the suspensions of CNCs and CAHNCs, respectively to be used as microscale models. In these Figures, changes in the color of images are related to changes in orientation direction of the nano and micro particle films against the polarized light. Figure 4a shows that CMCs are inherently turned and aligned perpendicular to the applied external magnetic field of 8 T; while, this magnetic intensity is not strong enough to effectively affect the starting diamagnetic CNCs and align them perpendicular to the applied external magnetic field direction. Therefore, because of random orientation of the CNCs against CMCs, the background color of the images in Figures 4aL and 4aR are exactly the same. As mentioned elsewhere by the authors, during the evaporation of liquid phase of the CNC suspension, especially if the CNCs are suspended in a polar liquid phase such as water, some disrupting physicochemical phenomena may play a role in preventing the magnetic alignment of the CNCs; interfacial interactions and surface tension forces are some of the most important preventing phenomena to be mentioned. Based on the PLM images shown here, the applied magnetic field intensity should be increased to values much higher than 8 T to successfully align the diamagnetic CNCs. On the other hand, PLM micrographs indicate that both the CAHMCs and CAHNCs were successfully aligned parallel to the magnetic field direction even under a magnetic field intensity of 2 T, in contrast with the inherent diamagnetic behavior of cellulose (Figures 4b and 4c). Investigation on the obtained PLM micrographs of the samples prepared in a magnetic field intensity of 1 T revealed that although this magnetic field intensity was not enough to well align the CAHNCs and

CAHMCs, the color distribution of images was different from those for the CNCs and CMCs. It seems that, under 1 T magnetic field intensity, some localized partial magnetic field induced self-assembly is formed, but the mentioned preventing forces partially disturbed the alignment quality.

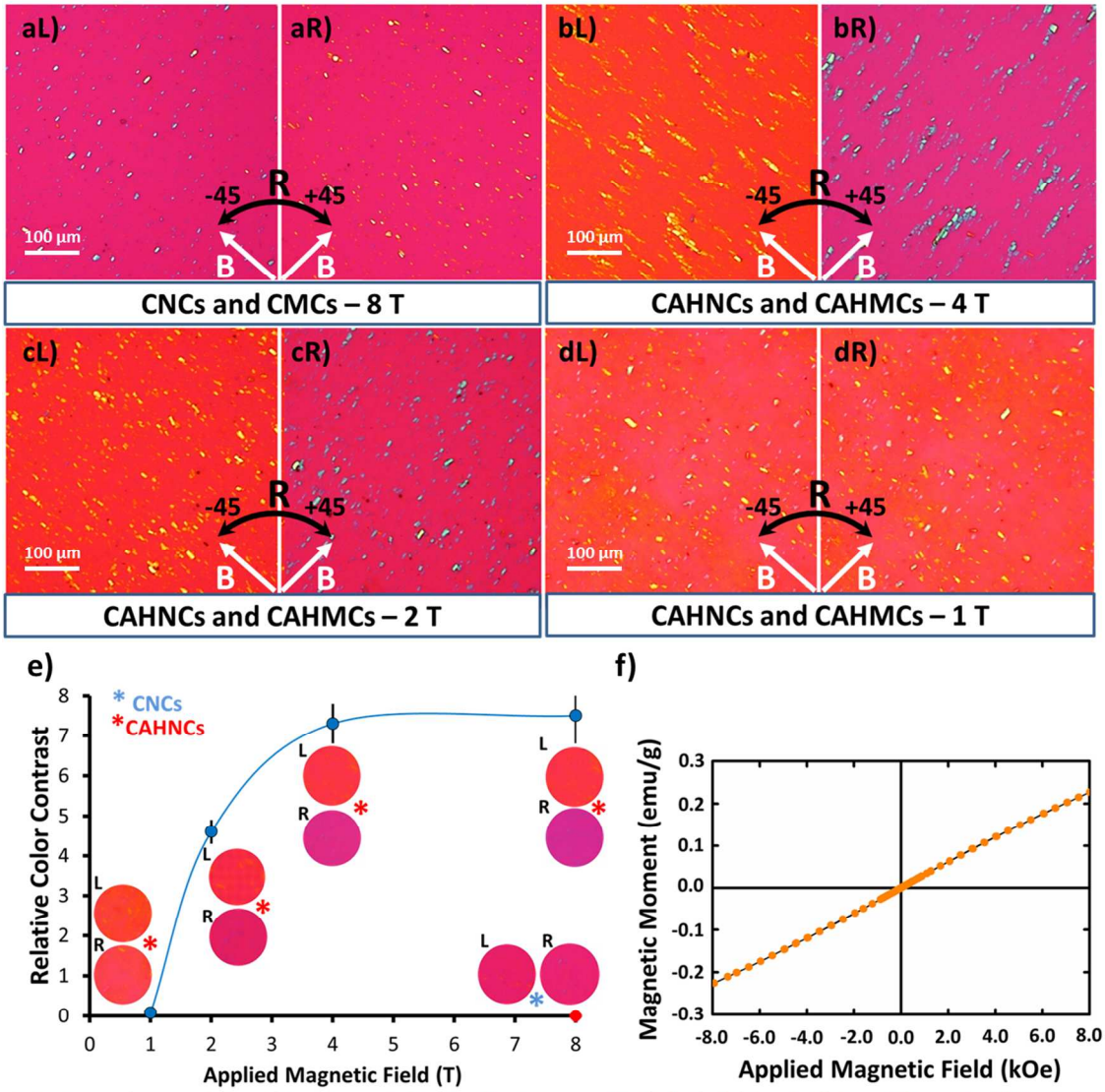

Figure 4. PLM observations of prepared films of the CNCs and CMCs under a static magnetic field of 8 T (aL and aR), the CAHNCs and CAHMCs under static magnetic fields of 4 T (bL and bR), 2 T (cL and cR), and 1 T (dL and dR) (The curved black arrows indexed by R indicate on rotation angles from -45° to +45°). e) The curve of RCC factor vs. the applied magnetic field intensity as a quantitative comparative criterion of the quality of the magnetic field induced self-assembly and orientation. f) The magnetic hysteresis loop for the synthetized CAHNCs at RT.

The other interesting phenomenon which can be seen in the captured PLM micrographs is the formation of some long and short well-ordered microstructures made of linearly magnetically assembled CAHMCs (Figure 4b and 4C). These linearly assembled microstructures are well aligned parallel to the external magnetic field direction. As PLM images show, with decreasing the applied magnetic field intensity, the length and frequency of these linearly assembled microstructures decrease. Such microstructures cannot be found in the case of prepared films from the diamagnetic CMCs and CNCs even by applying an 8 T magnetic field intensity (Figure 4a). Finally, by means of an innovative method, as mentioned in the experimental section, the difference of color contrast of the obtained PLM images were converted into quantitative values which are indexed as RCC factors. Figure 4e shows the relationship between the RCC factor and the applied magnetic field intensity. As seen, by increasing the magnetic field intensity from 1 T to 4 T, the RCC factor increases more than 7 times, but after that from 4 T to 8 T magnetic field intensity, the RCC factor shows no change. Thus, the magnetic field intensity of 4 T probably is quite adequate to achieve well aligned CAHNCs. Furthermore, no significant differences were observed between the estimated RCC factors of the prepared samples of diamagnetic CMCs and CNCs under 8 T and CAHMCs and CAHNCs under 1 T modulated magnetic field intensity.

To investigate the magnetic properties of the synthesized hybrid micro and nanoparticles, the magnetization of the samples was examined by means of a vibrating sample magnetometer (VSM). As Figure 4f shows, no hysteresis loop, coercivity, and retentivity were observed which indicate the superparamagnetic behavior of the synthesized akaganeite nanoparticles and of course the fabricated hybrid nano and microcrystals.

Figure 5a and 5b show FESEM micrographs of the unidirectionally aligned linearly self-assembled CAHMCs parallel to the applied external magnetic field of 4 T. Higher magnifications revealed that the present long linear configurations were composed of some linearly assembled shorter CAHMCs (Figure 5b). Figure 5c schematically explains probable causes of such well-aligned linear aggregations. It seems that the main reason is magnetic attraction among of the CAHMCs, which act like as 1D dipole micromagnets due to having a coverage of the superparamagnetic spherical akaganeite nanoparticles. In a strong enough external magnetic field, here 4 T, the spherical akaganeite nanoparticles act as single-domain magnetic nanoparticles due to having superparamagnetic properties. The orientation of the magnetic domain in each akaganeite nanoparticle is the same as the other, parallel to the external magnetic field direction. Therefore, each CAHMC can be envisioned as a 1D dipole micromagnet whose magnetic poles attract opposite poles of the neighboring CAHMC making the linear structures oriented in the direction of the applied external magnetic field.

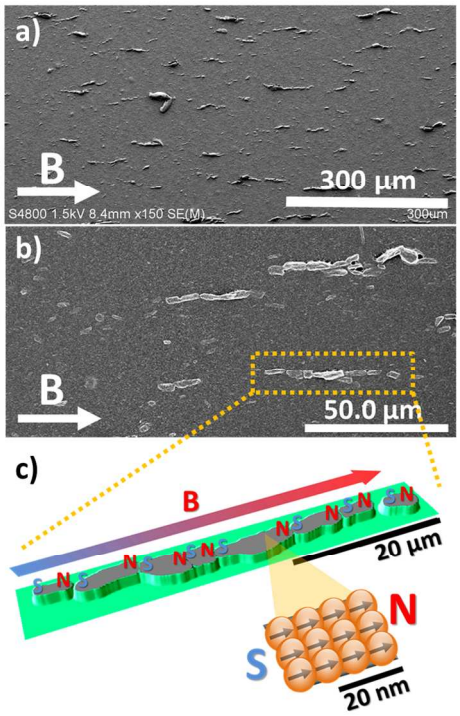

Figure 5. FESEM images of unidirectionally linear magnetic self-assembled CAHMCs under a magnetic field intensity of 4 T at different magnifications of a) X 150 and b) X 800. c) Schematic illustration of the magnetically self-assembled CAHMCs.

By comparing the obtained data from PLM and FESEM micrographs, it was found that the magnetic field intensity of 4 T was probably the optimal condition offering the highest level of alignment and orientation in this research. Figures 6a and 6b show PLM micrographs of the CAHNCs and CNCs, respectively, prepared from films obtained in the magnetic field of 4 T. These figures clearly indicate the successful unidirectional alignment of the CAHNCs and unsuccessful alignment of the diamagnetic CNCs by means of applying the external magnetic field of 4 T. FESEM micrographs strongly confirmed the PLM observations (Figures 6c and 6d).

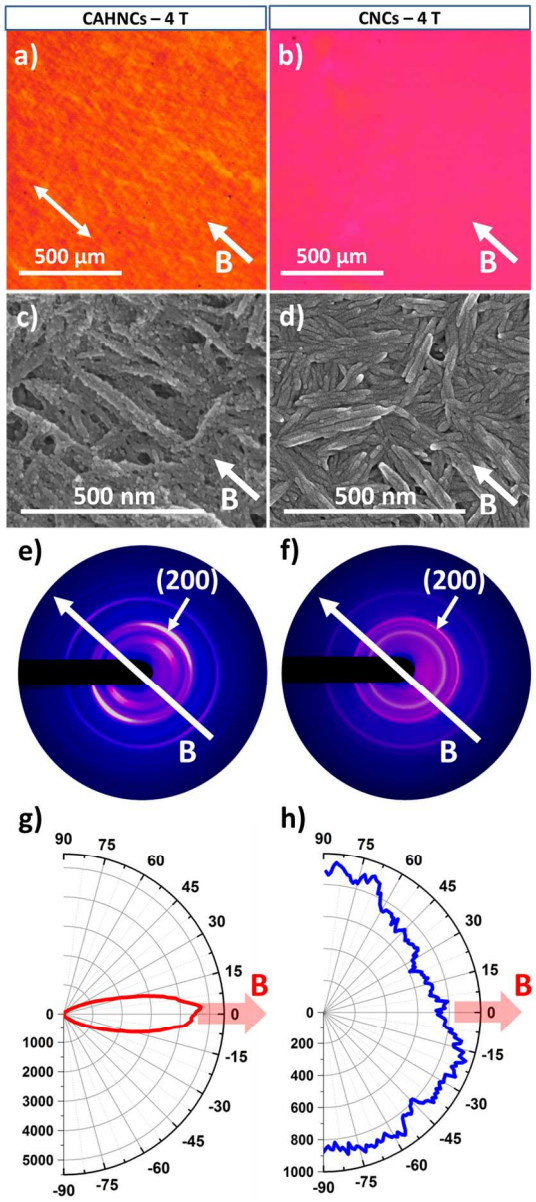

Figure 6. Results obtained from the characterization of the thin films of CAHNCs (left-handed images) and CNCs (right-handed images) made under a magnetic field of 4 T by means of PLM (a and b), FESEM (c and d), 2D WAXD (e and f), and polar scatter plots of orientation distribution of the CAHNCs (g) and CNCs (h) (vertical and angular axes, respectively show frequency and angle of the alignment)

2D X-ray diffraction imaging was performed to further confirm the obtained data from the FESM and PLM. Figure 6e clearly shows that, in the case of CAHNCs prepared under 4 T magnetic field intensity, the long axes of the hybrid nanocrystals are well aligned parallel to the magnetic field direction. On the contrary for the diamagnetic CNCs, the appearance the complete rings indicate random alignment of the CNCs independent of the direction of applied magnetic field (Figure 6F). Finally, to quantify the obtained data, image analysis was performed on the FESEM micrographs and the results can be seen in Figures 6g and 6h for the CAHNCs and CNCs, respectively. These polar scatter plots obviously indicate the high orientation of the CAHNCs parallel to the magnetic field of 4 T in contrast to the random distribution of alignment in the case of the CNCs.

CONCLUSIONS

In conclusion, we reported the first successful in situ synthesis of 1D cellulose akaganeite hybrid nanocrystals (CAHNCs) offering much higher magnetic response compared with the starting diamagnetic cellulose nanocrystals (CNCs). The reported fabrication process lead to direct conversion of the diamagnetic cellulose nanocrystals to the superparamagnetic CAHNCs composed of a core of crystalline cellulose and a shell of spherical akaganeite nanoparticles with the average particle size of 4 to 6 nm. As an important advantage, by using this method the challenge of the formation of extra magnetic nanoparticles and their separation is fully eliminated. The CAHNCs were well aligned even in an external magnetic field of 2 T whereas, the staring diamagnetic CNCs showed no alignment even under an 8 T magnetic field intensity. In addition, due to the akaganeite coverage, the easy axis of magnetization of the starting CNCs was changed from perpendicular to parallel to the magnetic field direction. Having organic-inorganic core shell structure, superparamagnetic behavior and relatively higher magnetic response make the CAHNCs a good candidate as high potential hybrid nanoparticles, which can be used in applications where having a hybrid structure at nanoscale and at the same time offering good magnetic response, biodegradability and renewability are important.

ACKNOWLEDGMENT

The authors are thankful to Mr. Mitsuhiko Morimoto and his colleagues of Perkin Elmer Japan Co., Ltd. Osaka Branch Office for the use of PerkinElmer Frontier spectrophotometer. Also, the authors gratefully acknowledge the financial support by the Graduate School of Agriculture, Kyoto University and the International Scientific Cooperation Office, Gorgan University of Agricultural Sciences and Natural Resources.

Notes and references

[a] Faculty of Wood and Paper Engineering, Gorgan University of Agricultural Sciences and Natural Resources, Gorgan, 49189-43464, Iran

[b] Fibrous Biomaterials Lab., Division of Forest and Biomaterials Science, Graduate School of Agriculture, Kyoto University, Kyoto, 606-8502, Japan

[c] School of Forest Resources, University of Maine, Orono, Maine, 04469, United States

1. Y. Xia, P. Yang, Y. Sun, Y. Wu, B. Mayers, B. Gates, Y. Yin, F. Kim and H. Yan, *Adv. Mater.*, 2003, 15, 353.
2. F. Kayaci, C. Ozgit-Akgun, I. Donmez, N. Biyikli and T. Uyar, *ACS Appl. Mater. Interfaces,* 2012, 4, 6185.
3. M. Macias-Montero, A. N. Filippin, Z. Saghi, F. J. Aparicio, A. Barranco, J. P. Espinos, F. Frutos, A. R. Gonzalez-Elipe and A. Borras, *Adv. Funct. Mater.*, 2013, 23, 5981.
4. Z. Sun, E. Zussman, A. L. Yarin, J. H. Wendorff and A. Greiner, *Adv. Mater.*, 2003, 15, 1929.
5. D. Zhang, L. Luo, Q. Liao, H. Wang, H. Fu and J. Yao, *J. Phys. Chem. C*, 2010, 115, 2360.
6. J. Kong, H. R. Tan, S. Y. Tan, F. Li, S. Y. Wong, X. Li and X. Lu, *Chem. Commun.*, 2010, 46, 8773.
7. M. Agrawal, A. Pich, S. Gupta, N. E. Zafeiropoulos, P. Simon and M. Stamm, *Langmuir*, 2008, 24, 1013.
8. X. Cui, S. Zhong and H. Wang, Polymer, 2007, 48, 7241.
9. H. Strohm and P. Löbmann, *Chem. Mater.*, 2005, 17, 6772.
10. Z. Liang, A. Susha and F. Caruso, Chem. Mater., 2003, 15, 3176.
11. L. A. Fielding and S. P. Armes, *J. Mater. Chem.*, 2012, 22, 11235.
12. K. Uetani and H. Yano, *Soft Matter*, 2013, 9, 3396.
13. Y. Habibi, L. A. Lucia and O. J. Rojas, Chem. Rev., 2010, 110, 3479.
14. J. P. Lagerwall, C. Schütz, M. Salajkova, J. Noh, J. H. Park, G. Scalia and L. Bergström, *NPG Asia Mater.*, 2014, 6, e80. doi:10.1038/am.2013.69
15. L. Rueda, A. Saralegi, B. Fernández-d'Arlas, Q. Zhou, A. Alonso-Varona, L. A. Berglund, I. Mondragon, M. Corcuera and A. Eceiza, *Cellulose*, 2013, 20, 1819.
16. R. Marchessault, P. Rioux and L. Raymond, *Polymer*, 1992, 33, 4024.
17. M. Mashkour, T. Kimura, F. Kimura, M. Mashkour and M. Tajvidi, *Biomacromolecules*, 2014, 15, 60.
18. J. Sugiyama, H. Chanzy and G. Maret, *Macromolecules*, 1992, 25, 4232.
19. T. Kimura, *Polym. J.*, 2003, 35, 823.
20. T. Kimura, H. Ago, M. Tobita, S. Ohshima, M. Kyotani and M. Yumura, *Adv. Mater.*, 2002, 14, 1380.
21. F. Kimura and T. Kimura, *Sci. Tech. Adv. Mater.*, 2008, 9, 024212.
22. F. Kimura, T. Kimura, M. Tamura, A. Hirai, M. Ikuno and F. Horii, *Langmuir*, 2005, 21, 2034.
23. S. T. Sundar, M. M. Sain and K. Oksman, *Carbohydr. Polym.*, 2010, 80, 35.
24. M. Mashkour, M. Tajvidi, T. Kimura, F. Kimura and G. Ebrahimi, *BioResources,* 2011, 6, 4731.
25. Z.-Y. Yuan and B.-L. Su, Chem. Phys. Lett., 2003, 381, 710-714.
26. H. Xiong, Y. Liao, L. Zhou, Y. Xu and S. Wang, *Environ. Sci. Technol.*, 2008, 42, 4165.
27. H. Fan, B. Song, Z. Yang and Q. Li, *Chem. Lett.*, 2004, 33, 576-577.
28. E. Murad and J. L. Bishop, *Am. Mineral.*, 2000, 85, 716.
29. S. Musić, S. Krehula and S. Popović, *Mater. Lett.*, 2004, 58, 444.